



Quantum Computation Based on Quantum Adiabatic Bifurcations of Kerr-Nonlinear Parametric Oscillators

Hayato Goto*

Corporate Research & Development Center, Toshiba Corporation, Kawasaki 212-8582, Japan

(Received August 30, 2018; accepted November 12, 2018; published online March 1, 2019)

Quantum computers with Kerr-nonlinear parametric oscillators (KPOs) have recently been proposed by the author and others. Quantum computation using KPOs is based on quantum adiabatic bifurcations of the KPOs, which lead to quantum superpositions of coherent states, such as Schrödinger cat states. Therefore, these quantum computers are referred to as “quantum bifurcation machines (QbMs)”. QbMs can be used for quantum adiabatic optimization and universal quantum computation. Superconducting circuits with Josephson junctions, Josephson parametric oscillators (JPOs) in particular, are promising for physical implementation of KPOs. Thus, KPOs and QbMs offer not only a new path toward the realization of quantum bits (qubits) and quantum computers, but also a new application of JPOs. Here we theoretically explain the physics of KPOs and QbMs, comparing them with their dissipative counterparts. Their physical implementations with superconducting circuits are also presented.

1. Introduction

Stimulated by commercial quantum computers developed by D-Wave systems,^{1–6)} which are based on quantum annealing^{7–10)} or adiabatic quantum computation,^{11–15)} hardware devices for combinatorial optimization have attracted much attention. D-Wave’s quantum annealers are Ising machines, that is, designed for finding ground states of the Ising model.¹⁶⁾ Since many combinatorial optimization problems can be mapped to the Ising problem,¹⁷⁾ fast Ising machines are expected to be useful for various real-world problems, including very-large-scale integrated (VLSI) circuit design,¹⁸⁾ computational biology,^{19–21)} classification problems,^{22,23)} scheduling or planning problems,^{24,25)} drug design,²⁶⁾ financial portfolio management,²⁷⁾ and traffic-flow optimization.²⁸⁾ Other kinds of Ising machines have also been proposed and developed using laser pulses,^{29–45)} electro-mechanical resonators,⁴⁶⁾ CMOS circuits,⁴⁷⁾ and magnetic devices.⁴⁸⁾

The first kind of laser-based Ising machine was proposed by Utsunomiya et al.²⁹⁾ and later developed by them.^{30–32)} This machine uses an injection-locked laser network and the “up” and “down” states of each Ising spin are represented by the polarizations^{29–31)} or phases³²⁾ of each mode. Importantly, Utsunomiya et al. introduced a new operational principle referred to as the *minimum-gain principle*.^{29,33)} The Ising energy (the cost function of the problem) is mapped to the total loss in the laser network. Then, the mode configuration with the minimum total loss requires the minimum gain for oscillation (the lowest threshold). Hence it oscillates most stably among all the configurations. Thus, we will obtain the ground state of the Ising model from the mode configuration of the steady state, assuming that the system chooses the most stable state with the minimum total loss as the steady state.

The second kind of laser-based Ising machine, which is called a *coherent Ising machine* (CIM), was proposed by Wang et al.³³⁾ and experimentally realized by them.³⁴⁾ This is also based on the minimum-gain principle, but uses a network of optical parametric oscillators (OPOs). An OPO is suitable for Ising machines, because it has two stable oscillating states above the threshold, which naturally represent an Ising spin. In other words, an OPO is an optical

implementation of the “parametron”.⁴⁹⁾ Large-scale CIMs have already been realized^{37,38)} using a measurement-feedback technique.^{39,40)}

Interestingly, the CIM searches an optimal solution in an opposite way to annealing approaches. That is, in contrast to annealing, the direction of the search in the CIM is “upward” in the energy landscape,³⁴⁾ where the gain is gradually increased and the lowest-threshold configuration is found.

The proposal of CIMs suggested parametric-oscillator implementations of Ising machines. Mahboob et al.⁴⁶⁾ proposed an Ising machine with electromechanical parametric resonators as a phononic counterpart of optical CIMs.

Since the minimum-gain principle inevitably requires losses, which usually result in decoherence, it seems difficult for machines based on this principle to harness quantum coherence, unlike standard quantum computers. To make the minimum-gain principle compatible with quantum coherence, Goto theoretically proposed an Ising machine composed of Kerr-nonlinear parametric oscillators (KPOs).⁵⁰⁾ A KPO is a parametric oscillator with large Kerr (or Duffing) nonlinearity and without losses in the ideal case. The Kerr (Duffing) nonlinearity is described by a quadratic (quartic) energy term with respect to oscillation power (amplitude). While in an OPO, the threshold is determined by one-photon loss and the oscillation is stabilized by two-photon loss, in a KPO, a detuning and the Kerr effect play the roles of the threshold and the stabilization, respectively. Since the detuning and the Kerr effect are described by their Hamiltonian terms, a KPO operates without dissipation and can maintain quantum coherence. A KPO is a nondissipative counterpart of an OPO.

A KPO can deterministically generate Schrödinger cat states^{51–60)} (quantum superpositions of coherent states) via quantum adiabatic evolution increasing the pumping rate gradually. Here, coherent states are eigenstates of annihilation operators⁵¹⁾ and regarded as the “most classical” states of light. The cat-state generation is understood as a result of a *quantum adiabatic bifurcation* of the KPO.⁵⁰⁾

By introducing nondissipative linear couplings between KPOs according to the coupling coefficients of a given Ising model, the Ising energy is approximately mapped to the threshold of the KPO network. Thus, the minimum-gain

principle is generalized to nondissipative oscillator networks. However, the two approaches rely on different mechanisms. In the case of an OPO network, the state of the system converges to an attractive steady state corresponding to a low Ising energy due to network losses. On the other hand, the KPO network has no losses and therefore has no attractive states. Instead, the KPO network can find the ground state of the Ising model via quantum adiabatic evolution increasing the pumping rate gradually. That is, convergence of the KPO network to an optimal solution is guaranteed by the quantum adiabatic theorem. This is called *bifurcation-based adiabatic quantum computation*,⁵⁰⁾ to distinguish it from conventional adiabatic quantum computation or quantum annealing, where quantum fluctuation terms are decreased gradually. (Puri et al.⁶¹⁾ reformulated adiabatic quantum computation using KPOs in a similar manner to quantum annealing.) Machines based on quantum adiabatic bifurcations of KPOs are called *quantum bifurcation machines* (QbMs)⁶²⁾ [with a lower-case “b” to distinguish this from quantum Boltzmann machines (QBM)s⁶³⁾].

KPOs that can generate cat states deterministically have not been experimentally realized to date. As suggested in Ref. 50, superconducting circuits with Josephson junctions are promising for implementing KPOs, because large Kerr effects can be realized using the nonlinearity of Josephson junctions^{64,65)} and parametric modulation can also be implemented easily by modulating the magnetic flux through a dc superconducting quantum interference device (SQUID).^{66–72)} Superconducting devices using such parametric modulation are known as Josephson parametric amplifiers (JPAs) or oscillators (JPOs). KPOs and QbMs offer a new application of JPOs. Nigg et al.⁷³⁾ and Puri et al.⁶¹⁾ proposed superconducting-circuit implementations for QbMs with *all-to-all connectivity*. The scheme proposed by Puri et al.⁶¹⁾ is particularly promising, which is based on the Lechner–Hauke–Zoller (LHZ) scheme^{74–76)} proposed for all-to-all connected quantum annealers. The four-body constraint required for the LHZ scheme, which is a technical difficulty in this scheme, is naturally realized by four-wave mixing in a Josephson junction. Using the technique to transform the four-body constraint to a three-body one,⁷⁷⁾ Zhao et al. proposed an alternative architecture.⁷⁸⁾

Single KPOs with small dissipation have been studied theoretically in the field of quantum nonlinear dynamics.^{79–81)} These studies have led to “quantum heating”, which is a heating process among quasienergy states by dissipation, where quasienergy states are eigenstates of the Hamiltonian in a rotating frame and in the rotating-wave approximation. Recently, Goto et al.⁶²⁾ generalized this concept from a single nonlinear oscillator to multiple coupled nonlinear oscillators through the study of dissipative QbMs. Consequently, it has been found that the distribution of the Ising energy becomes Boltzmann-like. More recently, this has been shown more directly by Dykman et al.⁸²⁾ This opens new possibilities for the application of QbMs, such as Boltzmann sampling for Boltzmann machine learning in the field of artificial intelligence.^{62,63,83)}

KPOs and QbMs have also opened new possibilities for standard gate-based quantum computers. After the proposal of the Ising machine with KPOs,⁵⁰⁾ Goto,⁸⁴⁾ and Puri et al.⁸⁵⁾ proposed gate-based universal quantum computation using

two oscillating states of a KPO as a qubit. (Other kinds of quantum computers with cat states or similar bosonic codes have also been proposed and developed.^{86–94)}) The fact that QbMs can perform universal quantum computation is significant, because it suggests that classical simulation of QbMs is extremely hard for the following reason. If QbMs are efficiently simulated using classical computers by any method, universal quantum computation can be simulated classically through QbM simulation. On the other hand, from quantum computational complexity theory, it is strongly believed that even non-universal quantum computation cannot be simulated classically.⁹⁵⁾ This leads to the hardness of classical simulation of QbMs. In contrast, there has not been such evidence for the hardness of classical simulation of CIMs so far.

In this paper, we describe the physics of KPOs and QbMs in comparison with OPOs and CIMs. Comparisons of a single KPO and a KPO network (QbM) with a single OPO and an OPO network (CIM) are summarized in Tables I and II, respectively. (The present models for an OPO and an OPO network are minimum ones for direct comparisons with a KPO and a KPO network. See Refs. 33–45 for more sophisticated or realistic models.) From these comparisons, KPOs and QbMs are nondissipative (imaginary) counterparts of OPOs and CIMs, respectively. The remainder of this paper is organized as follows. In Sect. 2, we describe the dynamics of a single KPO. In Sect. 3, we start with a summary of the theoretical aspects of a KPO network (QbM), and then we present simulation results for two coupled KPOs and four-spin Ising machines. In Sect. 4, we present superconducting-circuit implementations of a KPO and QbMs. In Sect. 5, we briefly explain how to realize a universal gate set for QbMs. Finally, a summary and outlook are provided in Sect. 6.

2. Physics of a KPO

In a frame rotating at half the pump frequency, $\omega_p/2$, and in the rotating-wave approximation, a quantum model of a KPO is given by the Schrödinger equation with the Hamiltonian \mathcal{H} in Table I,^{50,84)} where a^\dagger and a are the creation and annihilation operators, respectively, for the KPO. The Hamiltonian includes three terms corresponding to a Kerr effect, a detuning, and parametric pumping (two-photon driving). Here we assume a positive Kerr coefficient ($K > 0$). If $K < 0$ as in the case of Josephson parametric oscillators,^{61,67–73,85)} we redefine the Hamiltonian \mathcal{H} by flipping the overall phase, after which we obtain the same results. The detuning Δ is defined as $\Delta = \omega_{\text{KPO}} - \omega_p/2$, where ω_{KPO} is the one-photon resonance frequency of the KPO. Hereafter we assume $\Delta > 0$. This is a natural choice, because then the Kerr effect leads to larger detunings for larger amplitudes, and therefore stabilizes the oscillation. The case where $\Delta < 0$ is briefly discussed later. This corresponds to the case in Ref. 61, where the Kerr coefficient is negative and the detuning is positive.

A corresponding model for an OPO is given by the master equation in Table I, where the Kerr effect and the detuning are replaced by two-photon and one-photon losses, respectively. In the case of OPOs, the two-photon loss leads to larger losses for larger amplitudes, and thus stabilizes the oscillation. The phase of the pump amplitude is also

Table I. Comparison of a single KPO with a single OPO. \mathcal{H} and \mathcal{L} are the Hamiltonian for a KPO and the Liouvillian for an OPO, respectively. (We use the unit $\hbar = 1$.) p is the parametric pumping rate. K and Δ are the Kerr coefficient and the detuning, respectively, for the KPO. κ and κ_2 are the one-photon and two-photon loss rates, respectively, for the OPO. The classical models are defined with a complex amplitude $\alpha = x + iy$. H and E are the Hamiltonian for the classical KPO and the energy for the classical OPO, respectively. p_{th} denotes the thresholds (bifurcation points) for the classical models of the oscillators. “Oscillation amplitudes” are amplitudes corresponding to stable fixed points in the classical models.

	Single KPO	Single OPO
Quantum model	Schrödinger equation $ \dot{\psi}\rangle = -i\mathcal{H} \psi\rangle$ $\mathcal{H} = \frac{K}{2}a^{\dagger 2}a^2 + \Delta a^\dagger a - \frac{p}{2}(a^{\dagger 2} + a^2)$	Master equation $\dot{\rho} = \mathcal{L}\rho = -i[\mathcal{H}, \rho] + \mathcal{L}_1\rho + \mathcal{L}_2\rho$ $\mathcal{H} = i\frac{p}{2}(a^{\dagger 2} - a^2)$ $\mathcal{L}_1\rho = \kappa(2a\rho a^\dagger - a^\dagger a\rho - \rho a^\dagger a)$ $\mathcal{L}_2\rho = \frac{\kappa_2}{2}(2a^2\rho a^{\dagger 2} - a^{\dagger 2}a^2\rho - \rho a^{\dagger 2}a^2)$
	$\dot{\alpha} = i(p\alpha^* - \Delta\alpha - K \alpha ^2\alpha)$	$\dot{\alpha} = p\alpha^* - \kappa\alpha - \kappa_2 \alpha ^2\alpha$
	$\dot{x} = \frac{\partial H}{\partial y} = [p + \Delta + K(x^2 + y^2)]y$	$\dot{x} = -\frac{\partial E}{\partial x} = [p - \kappa - \kappa_2(x^2 + y^2)]x$
Classical model	$\dot{y} = -\frac{\partial H}{\partial x} = [p - \Delta - K(x^2 + y^2)]x$	$\dot{y} = -\frac{\partial E}{\partial y} = -[p + \kappa + \kappa_2(x^2 + y^2)]y$
	$H = -\frac{p}{2}(x^2 - y^2) + \frac{\Delta}{2}(x^2 + y^2) + \frac{K}{4}(x^2 + y^2)^2$	$E = -\frac{p}{2}(x^2 - y^2) + \frac{\kappa}{2}(x^2 + y^2) + \frac{\kappa_2}{4}(x^2 + y^2)^2$
	Threshold $p_{\text{th}} = \Delta$ (Detuning)	Threshold $p_{\text{th}} = \kappa$ (One-photon loss)
Stabilization	Kerr effect	Two-photon loss
Oscillation amplitudes	$\pm\sqrt{\frac{p - \Delta}{K}}$	$\pm\sqrt{\frac{p - \kappa}{\kappa_2}}$

Table II. Comparison of a KPO network (QbM) with an OPO network (CIM). $\mathcal{H}_i^{(1)}$ and $\mathcal{L}_i^{(1)}$ are the Hamiltonian for the i -th KPO and the Liouvillian for the i -th OPO, respectively, defined as \mathcal{H} and \mathcal{L} in Table I. \mathcal{H}_c and \mathcal{L}_c describe the couplings for KPOs and OPOs, respectively. $J_{i,j}$ is the coupling coefficient between the i -th and j -th Ising spins in a given Ising model. ξ_0 is a positive constant with the dimension of frequency. $H_i^{(1)}$ and $E_i^{(1)}$ are the classical Hamiltonian for the i -th KPO and the classical energy for the i -th OPO, respectively, defined as H and E in Table I. p_{th} denotes the thresholds (bifurcation points) for the classical models of the oscillator networks. λ_{\max} is the maximum eigenvalue of coupling matrix J .

	KPO network (QbM)	OPO network (CIM)
Quantum model	Schrödinger equation $ \dot{\psi}\rangle = -i\sum_{i=1}^N \mathcal{H}_i^{(1)} \psi\rangle - i\mathcal{H}_c \psi\rangle$ $\mathcal{H}_c = -\xi_0 \sum_{i=1}^N \sum_{j=1}^N J_{i,j}a_i^\dagger a_j$	Master equation $\dot{\rho} = \sum_{i=1}^N \mathcal{L}_i^{(1)}\rho + \mathcal{L}_c\rho$ $\mathcal{L}_c\rho = -\xi_0 \sum_{i=1}^N \sum_{j=1}^N J_{i,j}(2a_i\rho a_j^\dagger - a_j^\dagger a_i\rho - \rho a_j^\dagger a_i)$
	$\dot{\alpha}_i = i\left(p\alpha_i^* - \Delta\alpha_i - K \alpha_i ^2\alpha_i + \xi_0 \sum_{j=1}^N J_{i,j}\alpha_j\right)$	$\dot{\alpha}_i = p\alpha_i^* - \kappa\alpha_i - \kappa_2 \alpha_i ^2\alpha_i + \xi_0 \sum_{j=1}^N J_{i,j}\alpha_j$
	$\dot{x}_i = \frac{\partial H}{\partial y_i} = [p + \Delta + K(x_i^2 + y_i^2)]y_i - \xi_0 \sum_{j=1}^N J_{i,j}y_j$	$\dot{x}_i = -\frac{\partial E}{\partial x_i} = [p - \kappa - \kappa_2(x_i^2 + y_i^2)]x_i + \xi_0 \sum_{j=1}^N J_{i,j}x_j$
Classical model	$\dot{y}_i = -\frac{\partial H}{\partial x_i} = [p - \Delta - K(x_i^2 + y_i^2)]x_i + \xi_0 \sum_{j=1}^N J_{i,j}x_j$	$\dot{y}_i = -\frac{\partial E}{\partial y_i} = -[p + \kappa + \kappa_2(x_i^2 + y_i^2)]y_i + \xi_0 \sum_{j=1}^N J_{i,j}y_j$
	$H = \sum_{i=1}^N H_i^{(1)} - \frac{\xi_0}{2} \sum_{i=1}^N \sum_{j=1}^N J_{i,j}(x_i x_j + y_i y_j)$	$E = \sum_{i=1}^N E_i^{(1)} - \frac{\xi_0}{2} \sum_{i=1}^N \sum_{j=1}^N J_{i,j}(x_i x_j + y_i y_j)$
	Threshold $p_{\text{th}} = \Delta - \xi_0 \lambda_{\max}$	Threshold $p_{\text{th}} = \kappa - \xi_0 \lambda_{\max}$

redefined so that the oscillation phases are the same as those for the KPO.

Here we also introduce classical models⁵⁰⁾ corresponding to the quantum models, which are useful for grasping the dynamics of the oscillators. The classical models in Table I are derived as follows. Using the Schrödinger and master equations, we obtain

$$\text{KPO : } \langle \dot{a} \rangle = i(p\langle a^\dagger \rangle - \Delta\langle a \rangle - K\langle a^\dagger a^2 \rangle), \quad (1)$$

$$\text{OPO : } \langle \dot{a} \rangle = p\langle a^\dagger \rangle - \kappa\langle a \rangle - \kappa_2\langle a^\dagger a^2 \rangle, \quad (2)$$

where $\langle O \rangle$ represents the expectation value of an operator O and the dot denotes differentiation with respect to time t . These equations clearly show that the KPO is an imaginary counterpart of the OPO, and the detuning and the Kerr effect

correspond to the one-photon and two-photon losses, respectively. When the state is near to a coherent state $|\alpha\rangle$, moments are approximated as $\langle a^{\dagger m} a^n \rangle \approx \alpha^{*m} \alpha^n$, where the asterisk denotes complex conjugation. Thus, the classical models in Table I are derived from Eqs. (1) and (2).

The classical model for the KPO can be reformulated as a classical Hamiltonian dynamical system with the Hamiltonian H in Table I. Thus, H is conserved in this model, provided that the system parameters are constant. On the other hand, in the classical model for the OPO, the energy E in Table I of the same form as H decreases monotonically, because

$$\dot{E} \approx \frac{\partial E}{\partial x} \dot{x} + \frac{\partial E}{\partial y} \dot{y} = -(\dot{x}^2 + \dot{y}^2) < 0, \quad (3)$$

where the system parameters are assumed constant. Thus, the state of the OPO varies towards a local minimum of E .

We start with the discussion of the dynamics in the classical models to grasp the essence of these oscillators. Simulation results for the classical models of KPOs and OPOs are shown in Figs. 1(a) and 1(f), respectively. In these simulations, we set the parameters as $K = \Delta = 1$ and $\kappa_2 = \kappa = 1$ (K or κ_2 is the unit of frequency) and increase the pumping rate p linearly from 0 to 4 at the final time $t = 100$. The initial values are set as $x = y = 0.1$. In these figures, the dotted and dashed lines represent stable and unstable fixed points,⁹⁶⁾ respectively, where the fixed points are defined by $\dot{x} = \dot{y} = 0$. That is, the fixed points correspond to extrema of the Hamiltonian H or energy E . At $p = \Delta$ or $p = \kappa$, a single fixed point at the origin becomes two stable fixed points and an unstable fixed point, which is called a pitchfork bifurcation.⁹⁶⁾ Stable fixed points are given by the “oscillation amplitudes” in Table I. As shown in these figures, the system follows or converges to one of the two stable fixed points. In the case of an OPO, this is natural because the equations of motion lead to a monotonic decrease of E , and therefore the state approaches one of the local minima of E , which correspond to the stable fixed points. These dynamics are depicted in the phase portraits⁹⁶⁾ in Figs. 1(g) and 1(h), where the lines represent contours of E . On the other hand, the energy of the KPO is conserved and the state varies along a contour of H , as shown in Figs. 1(b) and 1(c). The dynamics of the KPO in Fig. 1(a) can be explained using an adiabatic invariant in classical mechanics.^{50,97–99)} The adiabatic invariant is defined as the area enclosed by the trajectory in the phase space. When p varies slowly, the adiabatic invariant is kept at a small value, which holds only near the local minima of the Hamiltonian. Consequently, the system follows one of them. We refer to this process as an *adiabatic bifurcation*.

Next, we perform similar simulations using the quantum models, where both the systems are initially in vacuum. The Wigner functions corresponding to the phase portraits are shown in Fig. 1, where filled and open circles represent stable and unstable fixed points, respectively, in the classical models. Here the Wigner function is a quasi-probability distribution defined as $W(\alpha) = \frac{2}{\pi} \text{Tr}[D(-\alpha)\rho D(\alpha)P]$ ^{50,51,56)} ($\alpha = x + iy$), where ρ is the density operator describing the system, $D(\alpha) = \exp(\alpha a^\dagger - \alpha^* a)$ is the displacement operator, and $P = \exp(i\pi a^\dagger a)$ is the parity operator. At the classical bifurcation points (thresholds), the two oscillators become similar squeezed states, as shown in Figs. 1(d) and 1(i). The large quantum fluctuations in the x direction may be useful when searching for optimal solutions in QbMs⁵⁰⁾ and CIMs.⁴⁵⁾

In the case of the OPO, the quantum state above the threshold is a mixed state of two coherent states corresponding to the classical stable fixed points, as shown in Fig. 1(j). This can be understood from the master equation as follows. When $\kappa = 0$, the master equation in Table I has exactly two steady states $|\pm\alpha_{SS}\rangle$, where $|\pm\alpha_{SS}\rangle$ are coherent states with $\alpha_{SS} = \sqrt{p/\kappa_2}$. When there exists small one-photon loss, coherence between the two states is lost due to the loss, and consequently the steady state becomes a mixed state of the two coherent states. The amplitudes become smaller due to the loss, which correspond to the classical stable fixed points (the “oscillation amplitudes” in Table I). (If the one-photon

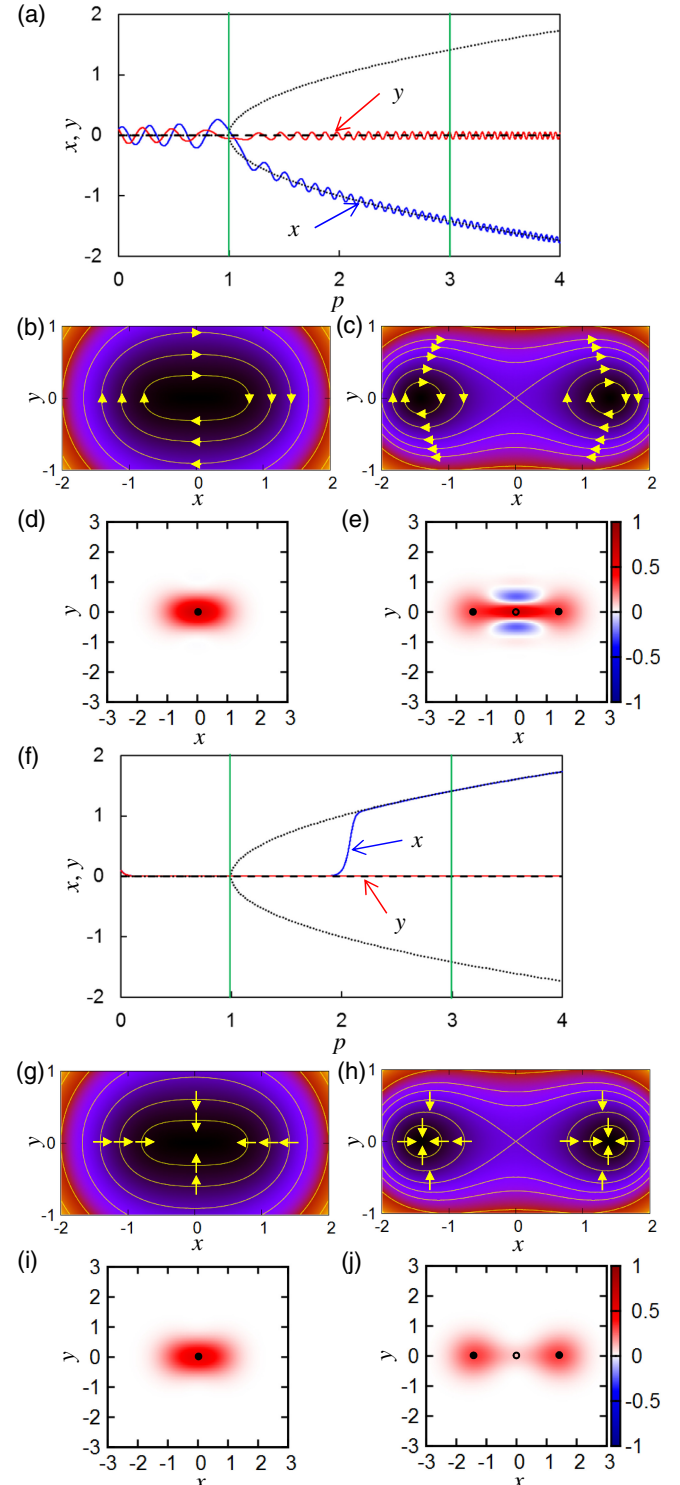


Fig. 1. (Color online) Simulation results for a KPO and an OPO. Parameters are set as $K = \Delta = 1$ and $\kappa_2 = \kappa = 1$ (K or κ_2 is the unit of frequency), and p is increased linearly from 0 to 4 at $t = 100$. (a) Time evolution of a classical KPO. (b) and (c) Phase portraits of the classical KPO at $p = 1$ (b) and $p = 3$ (c). (d) and (e) Wigner functions of the corresponding quantum KPO at $p = 1$ (d) and $p = 3$ (e). (f)–(j) are the corresponding results for an OPO. Stable and unstable fixed points in the classical models are represented, respectively, by the dotted and dashed lines in (a) and (f), and by the filled and open circles in the figures for the Wigner functions. Vertical lines in (a) and (f) indicate the values of p for the phase portraits and the Wigner functions.

loss is negligibly small, the relaxation due to the two-photon loss leads to steady cat states.¹⁰⁰⁾ This has been experimentally demonstrated using superconducting circuits.^{58,101)}

On the other hand, the Wigner function for a KPO above the threshold in Fig. 1(e) shows an interference fringe between two coherent states, which means that the two states are superposed. That is, a KPO above the threshold becomes an even cat state, $|\alpha_S\rangle + |-\alpha_S\rangle$, where $\pm\alpha_S$ correspond to the two classical stable fixed points (the “oscillation amplitudes” in Table I). Thus in quantum mechanics, the system follows two bifurcating branches “simultaneously”.⁵⁰⁾ This intriguing process is referred to as a *quantum adiabatic bifurcation*.

Its mechanism is explained as follows. For simplicity, we first assume no detuning. Then the Hamiltonian \mathcal{H} in Table I can be rewritten as

$$\mathcal{H} = \frac{K}{2} \left(a^{\dagger 2} - \frac{p}{K} \right) \left(a^2 - \frac{p}{K} \right), \quad (4)$$

where a c-number term has been dropped. Note that this is a positive semidefinite operator and that $\mathcal{H}|\pm\alpha_S\rangle = 0$. Hence the two coherent states are exactly degenerate ground states of \mathcal{H} . From the quantum adiabatic theorem, the final state becomes a ground state of the final Hamiltonian as long as the variation of p is sufficiently slow. Since the Hamiltonian is symmetric under the parity inversion $a \rightarrow -a$, parity is conserved. The vacuum state has even parity, and therefore we obtain the even cat state $|\alpha_S\rangle + |-\alpha_S\rangle$ via the quantum adiabatic evolution. When $\Delta > 0$, the vacuum state is a single ground state of the initial Hamiltonian. If the final value of p is large as compared to Δ , the detuning term can be treated as a perturbation. Assuming the final states are approximately composed of coherent states, the amplitudes are determined by the variational method minimizing the final energy.⁶²⁾ The resultant amplitudes are exactly the same as the stable fixed points of the classical model (the “oscillation amplitudes” in Table I). Again, the parity symmetry results in the even cat state with these amplitudes, as shown in Fig. 1(e).

Here we briefly discuss the case where $\Delta < 0$. As mentioned above, this corresponds to the case in Ref. 61). In this case, the Kerr effect decreases the detuning, and hence does not suppress oscillation amplitudes. Nevertheless, the Kerr effect stabilizes the oscillation after the amplitudes becomes sufficiently large. The simulation result for the Wigner function at $p = 3$ is shown in Fig. 2(a), where the parameter setting is the same as in Fig. 1 except for $\Delta = -1$. It turns out that we obtain a very intriguing state, instead of a cat state. (Based on the use of negative detunings, Zhang and Dykman¹⁰²⁾ theoretically proposed a method for preparation of quasienergy states other than cat states.)

However, if we set Δ to a smaller value like $\Delta = -0.2$, we can obtain an even cat state,⁶¹⁾ as shown in Fig. 2(b). This is understood as follows. In this case, the vacuum state is the first excited state of the initial Hamiltonian, whose ground state is the single-photon state. Since the quantum adiabatic theorem holds for any energy eigenstate, the even cat state is obtained via the adiabatic process following the first excited state. On the other hand, in the case where $\Delta = -1$, the vacuum state and the three-photon state are initially degenerate, which spoils the adiabatic cat-state generation.

In summary, in the case of negative detunings, we can control quantum states of a KPO via quantum adiabatic evolution, but it is necessary to carefully set the detuning to

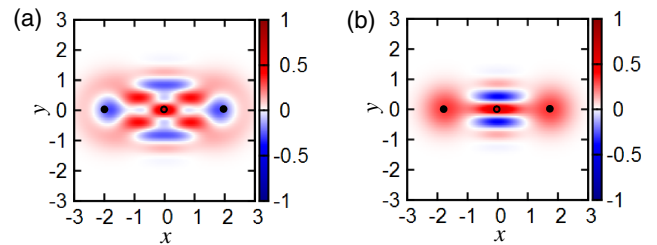


Fig. 2. (Color online) Simulation results for a KPO with a negative detuning. (a) and (b) Wigner functions at $p = 3$ with $\Delta = -1$ (a) and $\Delta = -0.2$ (b). Other parameters are set to the same values as in Fig. 1. Filled and open circles represent stable and unstable fixed points, respectively, in the classical model.

avoid degeneracy. This is unnecessary in the case of positive detunings.

3. KPO Network

3.1 Theory

Here we first explain how to introduce couplings between KPOs for solving the Ising problem using a KPO network (QbM). Next, we explain why the QbM can solve the Ising problem. Then, the corresponding explanations for an OPO network (CIM) are presented for comparison.

The Ising problem¹⁶⁾ requires finding the spin configuration that minimizes the following Ising energy:

$$E_{\text{Ising}}(\mathbf{s}) = -\frac{1}{2} \sum_{i=1}^N \sum_{j=1}^N J_{i,j} s_i s_j, \quad (5)$$

where s_i is the i -th Ising spin, which takes +1 (“up”) or -1 (“down”), N is the total number of the Ising spins, $\mathbf{s} = (s_1 s_2 \cdots s_N)$ is the vector representation of a spin configuration, and $J_{i,j}$ is the dimensionless coupling coefficient between the i -th and j -th spins ($J_{i,j} = J_{j,i}$ and $J_{i,i} = 0$). In this paper, for simplicity we do not consider local magnetic fields. See Refs. 26, 61, and 62 for their treatments.

In the case of a KPO network (QbM), the linear couplings described by the Hamiltonian \mathcal{H}_c in Table II are introduced,⁵⁰⁾ where a_i^\dagger and a_i are the creation and annihilation operators, respectively, for the i -th KPO and ξ_0 is a positive constant with the dimension of frequency.

To satisfy the condition that the vacuum state is the ground state of the initial Hamiltonian, we set ξ_0 such that the initial Hamiltonian is positive semidefinite. This is sufficient for the initial condition, because the pumping rate p is initially zero and then the vacuum state is a zero-eigenvalue eigenstate of the initial Hamiltonian. The condition is satisfied when $\Delta - \xi_0 \lambda_{\max} \geq 0$,⁵⁰⁾ where λ_{\max} is the maximum eigenvalue of the coupling matrix J , because then the detuning and coupling terms result in a positive semidefinite operator and the Kerr term is also positive semidefinite. The physical meaning of the linear couplings is photon exchange between two KPOs. This is easily implemented by coupling two KPOs directly or by using a far off-resonant coupling resonator. In the latter case, we can obtain the linear coupling Hamiltonian by adiabatically eliminating the resonator terms.

The corresponding classical model for the KPO network, which is provided in Table II, is derived in the same manner as in the single-KPO case. The bifurcation point (the threshold for the KPO network) in the classical model is given by $p_{\text{th}} = \Delta - \xi_0 \lambda_{\max}$.⁵⁰⁾ The above condition for a

positive semidefinite initial Hamiltonian in the quantum model corresponds to a nonnegative threshold in the classical model.

When solving the Ising problem, the pumping rate p is increased gradually from zero. Since the initial state is the ground state of the initial Hamiltonian as shown above, the final state will be the ground state of the final Hamiltonian according to the quantum adiabatic theorem, provided that the variation of p is sufficiently slow. The adiabatic condition is determined by the energy gap between the ground and first excited states.¹¹⁾ Thus, the energy-level structure of a KPO network is important, but has not been well understood yet.

If the final value of p is sufficiently large and the pumping and Kerr terms are dominant, the final state will be composed of coherent states, as in the single-KPO case. Thus, the final Hilbert space is approximately spanned by the N -mode coherent states $|s\rangle = |s_1\alpha_S\rangle \cdots |s_N\alpha_S\rangle$, where $\alpha_S = \sqrt{(p - \Delta)/K}$ and $s_j = \pm 1$ ($j = 1, \dots, N$). In this basis, the eigenvalues of the total Hamiltonian are given by

$$\langle s|H|s\rangle = \sum_{i=1}^N \left(\frac{K}{2} \alpha_S^4 + \Delta \alpha_S^2 - p \alpha_S^2 \right) - \xi_0 \alpha_S^2 \sum_{i=1}^N \sum_{j=1}^N J_{i,j} s_i s_j. \quad (6)$$

Note that the first term is constant and the second term is proportional to the Ising energy in Eq. (5). Therefore the ground state of the KPO network corresponds to the ground state of the Ising model. Thus, we obtain the solution of the Ising problem from the signs of the final amplitudes.

The Ising problem has two optimal solutions: S and $-S$. Correspondingly, the KPO network has degenerate ground states $|S\rangle$ and $|-\bar{S}\rangle$. Because of simultaneous parity symmetry of the total Hamiltonian,⁵⁰⁾ we obtain the entangled coherent states (multimode cat states) $|S\rangle + |-\bar{S}\rangle$ via the quantum adiabatic evolution from vacuum states.

In the case of an OPO network (CIM), couplings are implemented by mutual injection.³³⁾ (The measurement-feedback technique^{37–39)} is not considered in this paper.) In the classical model, mutual injection is modeled by adding terms proportional to the coupling coefficients,³³⁾ as shown in Table II. Then the total energy E in Table II decreases monotonically. Since E is of the same form as H for a KPO network, the threshold for the OPO network is given in a similar manner to that for the KPO network, as shown in Table II. When the pumping rate p is sufficiently large, the variables for the steady state are approximated as $x_j \approx s_j x_{SS}$ and $y_j \approx 0$, where $x_{SS} = \sqrt{(p - \kappa)/\kappa_2}$ and $s_j = \pm 1$. Then, the first term in E is constant and the second term in E is proportional to the Ising energy. Hence, the signs of the x values for the steady state provide an approximate solution of the Ising problem.

The corresponding quantum model is given by the master equation in Table II. This is reformulated in the standard Lindblad form¹⁰³⁾ as follows:

$$\dot{\rho} = -i[\mathcal{H}, \rho] + \mathcal{L}_1 \rho + \mathcal{L}_2 \rho + \mathcal{L}_3 \rho, \quad (7)$$

$$\mathcal{H} = i \frac{p}{2} \sum_{i=1}^N (a_i^{\dagger 2} - a_i^2), \quad (8)$$

$$\mathcal{L}_1 \rho = \sum_{i=1}^N \left(\kappa - \xi_0 \sum_{j=1}^N |J_{i,j}| \right) (2a_i \rho a_i^{\dagger} - a_i^{\dagger} a_i \rho - \rho a_i^{\dagger} a_i), \quad (9)$$

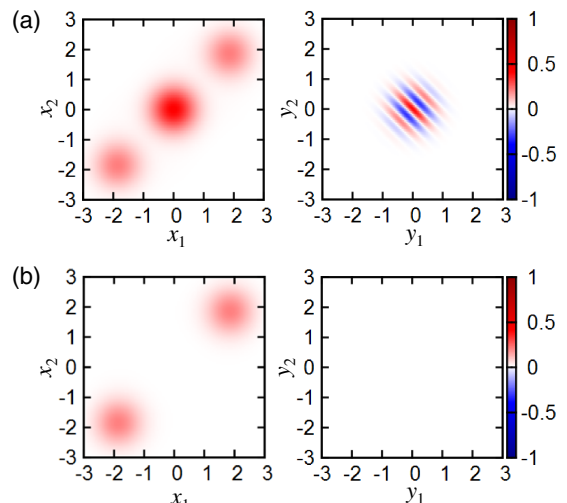


Fig. 3. (Color online) Simulation results for the quantum models of two coupled oscillators. (a) Two-mode Wigner function for KPOs at the final time. Left: $y_1 = y_2 = 0$. Right: $x_1 = x_2 = 0$. (b) Corresponding results for OPOs. Parameter setting: $J_{1,2} = J_{2,1} = 1$, $\xi_0 = 0.5$, and others are set to the same values as in Fig. 1.

$$\mathcal{L}_2 \rho = \sum_{i=1}^N \frac{\kappa_2}{2} (2a_i^2 \rho a_i^{\dagger 2} - a_i^{\dagger 2} a_i^2 \rho - \rho a_i^{\dagger 2} a_i^2), \quad (10)$$

$$\mathcal{L}_3 \rho = \sum_{i=1}^N \sum_{j=1}^{i-1} \xi_0 |J_{i,j}| (2L_{i,j} \rho L_{i,j}^{\dagger} - L_{i,j}^{\dagger} L_{i,j} \rho - \rho L_{i,j}^{\dagger} L_{i,j}), \quad (11)$$

where the Lindblad operators for the couplings are defined as $L_{i,j} = a_i - \frac{J_{i,j}}{|J_{i,j}|} a_j$. This is implemented by using lossy injection paths,⁴²⁾ where adiabatic elimination of the injection-path terms leads to the Lindblad operators. This is a fully quantum-mechanical model for an OPO network (CIM).

Interestingly, the classical models can also find good solutions of the Ising problem with high probability,⁵⁰⁾ as shown in Fig. 4 later. This is because in the two classical models, the x values become the maximum-eigenvalue eigenvector of the coupling matrix J at the threshold, which provides an approximate solution of the Ising problem.⁵⁰⁾ This is easily understood from the fact that the Ising energy in Eq. (5) is a quadratic form with the coefficient matrix $-J$. This is an explanation of the minimum-gain principle from a classical point of view. However, the x values are continuous, unlike Ising spins, and hence their dispersion induces errors (trapping at a wrong configuration). In the quantum model of the QbM, quantum fluctuations lead to a superposition of many spin configurations at the threshold, and consequently the system escapes from the trap. This results in higher performance of the quantum model of the QbM than the classical counterpart⁵⁰⁾ (see Fig. 4).

3.2 Two coupled oscillators

As a simplest example of the Ising problem, here we consider two coupled oscillators for a two-spin Ising model with ferromagnetic coupling, whose ground states are $s_1 = s_2 = 1$ and $s_1 = s_2 = -1$.

Simulation results using the quantum models are shown in Fig. 3. In this simulation, we set $J_{1,2} = J_{2,1} = 1$ and $\xi_0 = 0.5$, and the other parameters are set to the same values as in Fig. 1. Figures 3(a) and 3(b) show the two-mode Wigner

functions for the two KPOs and the two OPOs, respectively, at the final time. Here, the two-mode Wigner function is defined as $W(\alpha_1, \alpha_2) = (\frac{2}{\pi})^2 \text{Tr}[D_1(-\alpha_1)D_2(-\alpha_2)\rho D_1(\alpha_1) \times D_2(\alpha_2)P_1P_2]$,⁵⁹⁾ where D_i and P_i are the displacement and parity operators for the i -th oscillator, respectively. To display the two-mode Wigner functions with four variables, we set $y_1 = y_2 = 0$ in the left figures and $x_1 = x_2 = 0$ in the right figures in Fig. 3.

The two peaks around $x_1 = x_2 = 2$ and -2 correspond to the ground states of the Ising model. That is, both models successfully find the solutions. However, there are apparent differences around the origin. There is nothing around the origin in the case of OPOs. This means that the final state of the two OPOs is a mixed state of two-mode coherent states. On the other hand, there is an interference fringe for KPOs. This shows that the final state of the two KPOs is an entangled coherent state (two-mode cat state), as expected. Such Wigner functions have recently been experimentally observed using two microwave cavities coupled to a Y-shaped superconducting qubit⁵⁹⁾ by a different technique.

3.3 Four-spin Ising machines

So far, we have considered four oscillator-network models (KPO/OPO and quantum/classical). Hereafter, we use the following abbreviations: “qQbM” and “cQbM” represent the quantum and classical models, respectively, for QbMs (KPO networks); “qCIM” and “cCIM” represent the quantum and classical models, respectively, for CIMs (OPO networks).

To evaluate the performances of the four models, we perform numerical simulation for the four-spin Ising problem with all-to-all connectivity. We solve 100 instances using the four models, where the coupling coefficients $\{J_{i,j}\}$ for each instance are set randomly from among the 21 values $\{-1, -0.9, \dots, 1\}$. In this simulation, $\xi_0 = 0.25$ and other parameters are set to the same values as in Figs. 1 and 3.

For the qQbM simulation, we numerically solve the Schrödinger equation in Table II. In the qCIM simulation, we use a Monte Carlo simulation called the quantum jump (or trajectory) approach^{103–105)} for the Lindblad-form master equation given by Eqs. (7)–(11), instead of solving the master equation directly. This approach, which is applicable to any Lindblad-form master equation, uses a state vector, instead of a density matrix, and its implementation is therefore easier and consumes less memory. We repeat the Monte-Carlo simulation 20 times, and take their average result. To simulate the classical models, we numerically solve the equations of motion in Table II 10^3 times with initial values set randomly within the interval $(-0.1, 0.1)$, and take their average result.

The simulation results are shown by the histograms in Fig. 4, where the probabilities for spin configurations in the quantum models are calculated using the formula in Ref. 50. Comparing Figs. 4(a)–4(d), we conclude that the qQbM achieves the best performance among the four models. The high performance of the qQbM as compared with the cQbM is explained by quantum fluctuations and quantum superpositions, which help the qQbM to escape from local minima.⁵⁰⁾

On the other hand, the performance of the qCIM is remarkably low. This is due to quantum noises (quantum jumps) from one-photon losses in OPOs and injection paths.

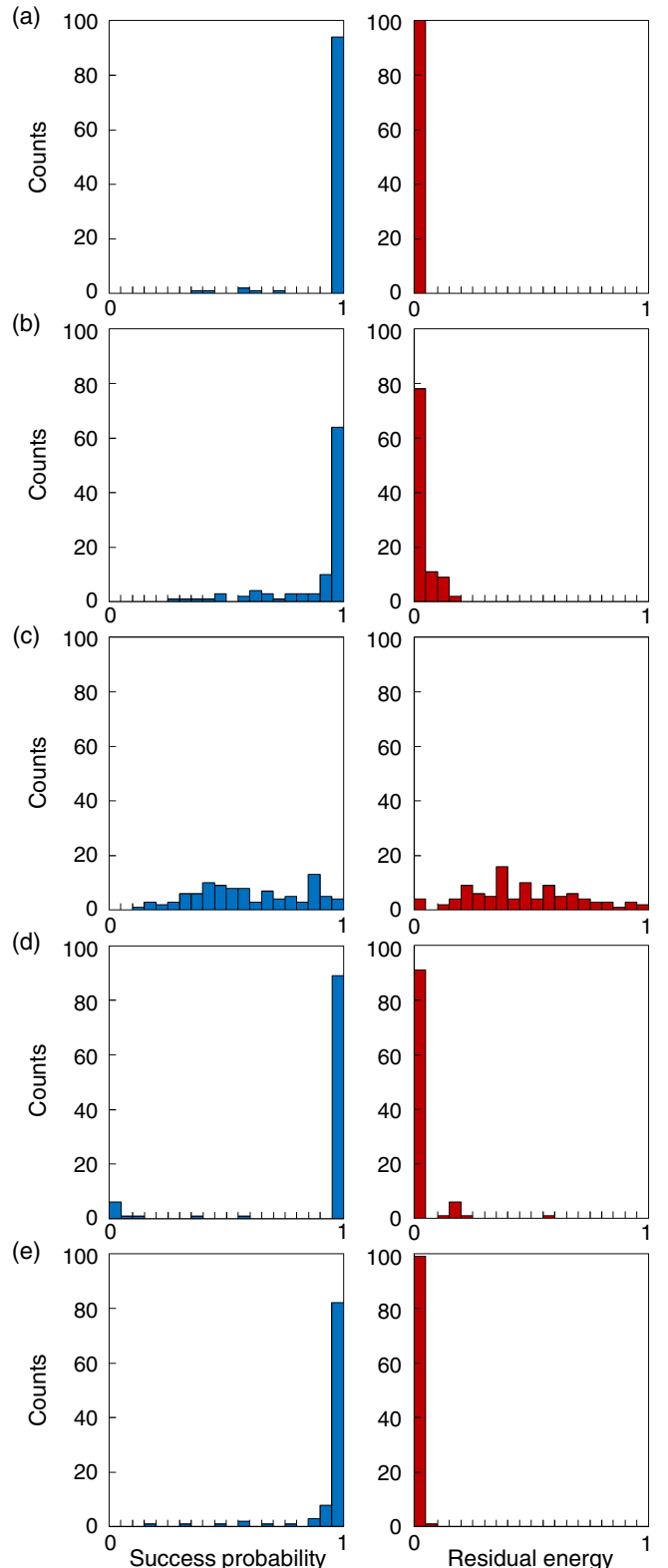


Fig. 4. (Color online) Simulation results for four-spin Ising machines. (a) qQbM. (b) cQbM. (c) qCIM. (d) cCIM. (e) qCIM without quantum jumps due to one-photon losses in OPOs and injection paths. Left: Success probability for obtaining the ground states. Right: Residual energy (difference between the average Ising energy obtained in the simulations and the ground-state energy). Parameter setting: $\xi_0 = 0.25$, $\{J_{i,j}\}$ are set randomly from among $\{-1, -0.9, \dots, 1\}$, and others are set to the same values as in Figs. 1 and 3.

In fact, its performance becomes much higher under the condition that no such quantum jumps occur, as shown in Fig. 4(e). (This is an unrealistic illustrative situation for

observing the effects of the quantum noise.) This result indicates that it is hard to exploit quantum coherence in CIMs. In contrast, the performance of the cCIM is surprisingly high. This may be because the cCIM can successfully follow one of local minima of its energy, which leads to a low Ising energy. This result indicates that the classical regime is preferable for CIMs to the quantum regime. For some instances, however, the cCIM almost always fails, as shown by very low success probabilities in Fig. 4(d). This result comes from the fact that the cCIM is sometimes trapped by a nonglobal local minimum.

The high performance of the qQbM is achieved assuming no loss in the KPO network. Such loss induces quantum heating, and consequently the probability distribution of the Ising energy becomes Boltzmann-like.^{62,82)} This result offers two good possibilities: QbMs can provide good approximate solutions with high probabilities even in the presence of loss; dissipative QbMs will be useful for Boltzmann sampling from the Ising model. It is an open question whether such computations provide a speedup over classical computations.

4. Superconducting-circuit Implementations

KPOs that can generate cat states have not been experimentally realized so far. A condition for this realization is negligibly small dissipation relative to the Kerr coefficient and a parametric pumping rate, which would be difficult to realize in optical or mechanical systems. Superconducting circuits with Josephson junctions are natural candidates and the most promising for realizing such low-loss KPOs. Here, we explain how a KPO and Ising machines with KPOs (QbMs) are implemented with superconducting circuits.^{61,73,78)}

4.1 Implementation of a KPO

As a simplest model for a KPO, here we consider a frequency-tunable transmon qubit, an equivalent circuit of which is shown in Fig. 5. Transmons^{106–116)} are widely used superconducting qubits, which are composed of a capacitor with large capacitance C and a Josephson junction characterized by a critical current I_c . Since a Josephson junction can be regarded as a nonlinear inductor with $L_J = \phi_0/(I_c \cos \varphi)$,¹¹⁷⁾ the transmon is a LC resonator with anharmonicity, where $\phi_0 = \Phi_0/(2\pi) = \hbar/(2e)$ is the reduced flux quantum (Φ_0 is the flux quantum) and φ is the phase difference across the junction. The large capacitance of a transmon leads to a charging energy $E_C = e^2/(2C)$ that is smaller than a Josephson energy $E_J = I_c \phi_0$, making it insensitive to charge noises. By replacing the Josephson junction with a dc SQUID (a loop with two identical Josephson junctions), the critical current can be controlled by the magnetic flux Φ through the dc SQUID as $\tilde{I}_c = 2I_c \cos(\pi\Phi/\Phi_0)$,^{118,119)} where \tilde{I}_c denotes the effective critical current for a dc SQUID. Thus, the resonance frequency of the transmon can be controlled by the flux bias.

The Hamiltonian for the transmon is given by^{106,117,119)}

$$H = \frac{Q^2}{2C} - \tilde{E}_J \cos \varphi, \quad (12)$$

where Q is the capacitor charge and $\tilde{E}_J = \tilde{I}_c \phi_0$ is the effective Josephson energy for the dc SQUID. φ and Q satisfy the commutation relation $[\varphi, Q] = i(2e)$.¹¹⁷⁾ In fact, using this,

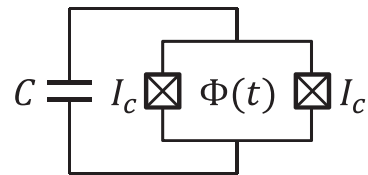


Fig. 5. Equivalent circuit for a frequency-tunable transmon qubit. C : Shunt capacitance for the transmon. I_c : Critical current for each Josephson junction of the dc SQUID. $\Phi(t)$: Magnetic flux through the dc SQUID.

their Heisenberg equations of motion reproduce the ac and dc Josephson relations^{117,118)} as follows:

$$\frac{Q}{C} = \phi_0 \dot{\varphi}, \quad -\dot{Q} = \tilde{I}_c \sin \varphi. \quad (13)$$

In the transmon regime ($E_C \ll \tilde{E}_J$), the phase difference is confined at the bottom of the potential, that is, $\langle \varphi^2 \rangle \ll 1$. Therefore, we use the approximation $\cos \varphi \approx 1 - \frac{\varphi^2}{2} + \frac{\varphi^4}{24}$. Here the dc and ac parts of the flux are defined as

$$\Phi(t) = \Phi^{dc} + \Phi^{ac}(t), \quad \Phi^{ac}(t) = \delta_p \Phi_0 \cos \omega_p t,$$

where δ_p and ω_p denote the amplitude and frequency, respectively, of the modulation for parametric pumping. When $\delta_p \ll 1$, the Hamiltonian in Eq. (12) is approximated as

$$\begin{aligned} H &\approx \frac{Q^2}{2C} + \frac{\tilde{E}_J^{dc}}{2} \varphi^2 + \frac{\tilde{E}_J^{ac}(t)}{2} \varphi^2 - \frac{\tilde{E}_J^{dc}}{24} \varphi^4, \\ \tilde{E}_J^{dc} &\approx 2E_J \cos\left(\pi \frac{\Phi^{dc}}{\Phi_0}\right), \\ \tilde{E}_J^{ac}(t) &\approx -2\pi\delta_p E_J \sin\left(\pi \frac{\Phi^{dc}}{\Phi_0}\right) \cos \omega_p t. \end{aligned} \quad (14)$$

Note that the first and second terms in Eq. (14) describe a harmonic oscillator. Hence φ and Q are expressed with creation and annihilation operators as

$$\varphi = \left(\frac{2E_C}{\tilde{E}_J^{dc}}\right)^{\frac{1}{4}} (a + a^\dagger), \quad Q = ie\left(\frac{\tilde{E}_J^{dc}}{2E_C}\right)^{\frac{1}{4}} (a^\dagger - a). \quad (15)$$

Substituting these into Eq. (14) and disregarding c-number terms, the Hamiltonian in a frame rotating at $\omega_p/2$ and in the rotating-wave approximation is given by the KPO Hamiltonian in Table I with the following parameters:

$$\hbar\Delta = \sqrt{8E_C\tilde{E}_J^{dc}} - E_C - \hbar \frac{\omega_p}{2}, \quad (16)$$

$$\hbar K = -E_C, \quad (17)$$

$$\hbar p = \pi\delta_p E_J \sin\left(\pi \frac{\Phi^{dc}}{\Phi_0}\right) = \frac{\pi\delta_p \tilde{E}_J^{dc}}{2} \tan\left(\pi \frac{\Phi^{dc}}{\Phi_0}\right), \quad (18)$$

where \hbar is shown explicitly. It is notable that the Kerr coefficient is determined only by the charging energy E_C ¹⁰⁶⁾ and the one-photon resonance frequency ω_{KPO} is approximately given by the Josephson plasma frequency $\sqrt{8E_C\tilde{E}_J^{dc}/\hbar}$.^{106,118)}

From Eqs. (17) and (18), the average photon number for the parametric oscillation with $\Delta = 0$, n_{ave} , is expressed as

$$n_{ave} = \left| \frac{p}{K} \right| \approx \frac{\pi\delta_p}{16} \left(\frac{\omega_{KPO}}{K} \right)^2 \left| \tan\left(\pi \frac{\Phi^{dc}}{\Phi_0}\right) \right|, \quad (19)$$

where $\hbar\omega_{\text{KPO}} \approx \sqrt{8E_C\tilde{E}_J^{\text{dc}}}$ has been used. Since δ_p is a small modulation amplitude, $\delta_p \ll 1$, n_{ave} is upper bounded by the right-hand side of Eq. (19) divided by δ_p . On the other hand, n_{ave} is also upper bounded by the condition $\langle\varphi^2\rangle \ll 1$. Using Eq. (15), this condition is rewritten as

$$\langle\varphi^2\rangle \approx \sqrt{\frac{2E_C}{\tilde{E}_J^{\text{dc}}}(4|\alpha|^2 + 1)} \ll 1 \Rightarrow n_{\text{ave}} = |\alpha|^2 \ll \frac{\omega_{\text{KPO}}}{16|K|},$$

assuming a coherent state with amplitude $\alpha = \sqrt{n_{\text{ave}}}$. Both the upper bounds indicate that large n_{ave} requires large $\omega_{\text{KPO}}/|K|$. For typical transmon qubits,¹¹⁵⁾ $\omega_{\text{KPO}}/(2\pi) \approx 5 \text{ GHz}$ and $|K|/(2\pi) \approx 200 \text{ MHz}$, and therefore $\omega_{\text{KPO}}/(16|K|) \approx 1.6$. This value is too small for parametric oscillations. This indicates that a larger capacitance and a larger critical current are desirable for the implementation of a KPO.

4.2 Architectures for QbMs

Here we present two proposed architectures for QbMs.^{61,73)} Nigg et al.⁷³⁾ proposed the KPO-ring architecture shown in Fig. 6 for QbMs with all-to-all connectivity. Antiferromagnetic coupling, which is required for interesting problems, is realized by setting the flux bias as $\Phi_e = \Phi_0/2$ or by shunting the ring with a π -junction.^{120–122)} In this scheme, the coupling coefficients are given by $J_{i,j} \propto \sqrt{Z_i Z_j}$, where Z_i is the mode impedance for the i -th KPO. Thus, this scheme has only N tunable parameters $\{Z_1, \dots, Z_N\}$, not all $N(N - 1)/2$ patterns. Nevertheless, this can be used for hard problems such as the number partitioning problem, which is an NP-hard combinatorial optimization problem in which N numbers $\{n_1, \dots, n_N\}$ are partitioned into two groups such that the sum of one group is equal to that of the other. The number partitioning problem is equivalent to the Ising problem with $J_{i,j} \propto n_i n_j$,¹⁷⁾ which can be treated in this scheme. To tune mode impedances to desired values without changing the mode frequencies, Nigg et al. proposed the use of tunable capacitors. A scheme to extend the connectivity from $O(N)$ to $O(N \log N)$ has also been proposed (see the Supplementary Materials in Ref. 73).

Another QbM architecture with all-to-all connectivity was proposed by Puri et al.⁶¹⁾ using the LHZ scheme.⁷⁴⁾ A conventional approach to all-to-all connected quantum annealers is “minor embedding”.^{123,124)} The LHZ scheme was proposed as an alternative approach to all-to-all connected quantum annealers for realizing a fully two-dimensional layout of qubits with only nearest-neighbor interactions. In the LHZ scheme, each physical qubit represents the product of two Ising spins, instead of an individual Ising spin. Therefore, this scheme is also called parity adiabatic quantum computing (PAQC).⁷⁷⁾ Coupling coefficients are introduced as local fields for the physical qubits, and hence can be controlled more easily than real coupling strengths between qubits. Corresponding to the coupling coefficients, this scheme needs $N(N - 1)/2$ physical qubits. The additional degrees of freedom is reduced by four-body constraints among four adjacent qubits, where the eigenvalue of the four-qubit Pauli-Z operator must be one.⁷⁴⁾ This is a technical obstacle for the LHZ scheme.⁷⁶⁾

Remarkably, the four-body constraint is easily implemented for KPOs by four-wave mixing in a Josephson junction coupled to four adjacent KPOs, as shown in

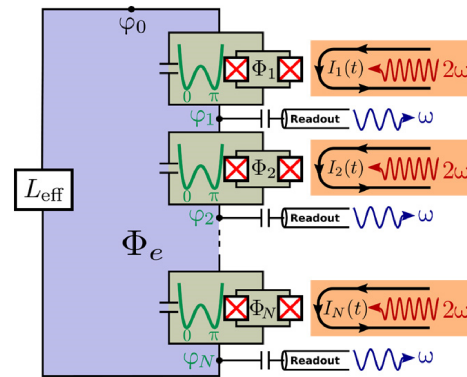


Fig. 6. (Color online) KPO-ring architecture for QbM with all-to-all connectivity. Adapted from Ref. 73 under the CC BY-NC 4.0 license.

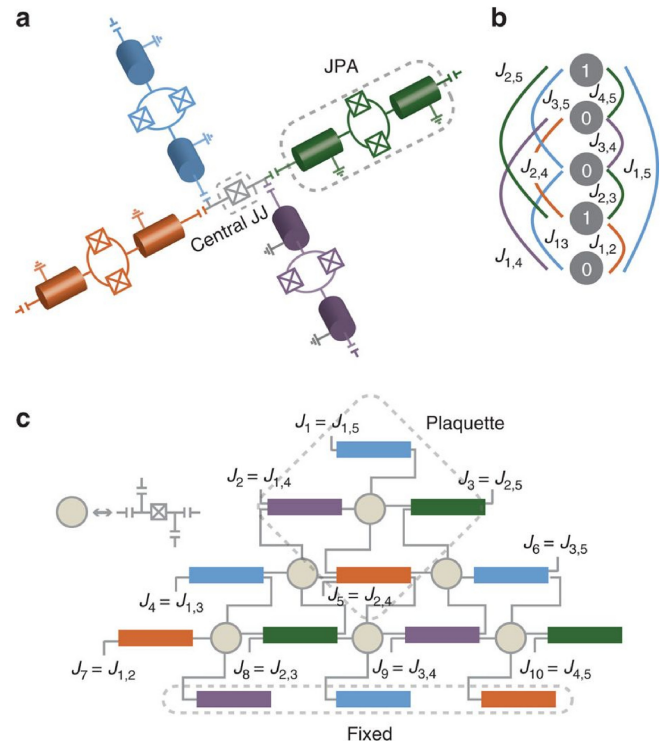


Fig. 7. (Color online) QbM architecture based on the LHZ scheme. Adapted from Ref. 61 under the CC BY 4.0 license.

Fig. 7(a). When the four KPOs have different resonance frequencies and a four-photon resonance condition, e.g., $\omega_1 + \omega_2 = \omega_3 + \omega_4$ is satisfied, the four-body interaction yields only terms such as $a_1^\dagger a_2^\dagger a_3 a_4$ in the rotating-wave approximation. These result in the four-body constraint in the coherent-state basis.⁶¹⁾

5. Universal Quantum Computation Using KPOs

A KPO network (QbM) can also be used for gate-based universal quantum computation,^{84,85)} where a qubit is represented by two oscillating states, $|\pm\alpha_S\rangle$, of each KPO. Although $|\bar{0}\rangle = |\alpha_S\rangle$ and $|\bar{1}\rangle = |-\alpha_S\rangle$ are not orthogonal to each other, the inner product $\langle -\alpha_S | \alpha_S \rangle = e^{-2\alpha_S^2}$ is negligible for large α_S , and hence they can be used for computational-basis states. Here we briefly explain how to realize a universal gate set for the coherent-state qubits.

A universal gate set is composed of two kinds of single-qubit rotation, $R_Z(\phi)$ and $R_X(\theta)$, and a two-qubit gate, $U_{ZZ}(\Theta)$, which are defined as follows:^{84,125}

$$R_Z(\phi)(\alpha_0|\bar{0}\rangle + \alpha_1|\bar{1}\rangle) = \alpha_0 e^{-i\phi/2}|\bar{0}\rangle + \alpha_1 e^{i\phi/2}|\bar{1}\rangle,$$

$$R_X(\theta)(\alpha_0|\bar{0}\rangle + \alpha_1|\bar{1}\rangle) = \left(\alpha_0 \cos \frac{\theta}{2} - i\alpha_1 \sin \frac{\theta}{2} \right)|\bar{0}\rangle + \left(\alpha_1 \cos \frac{\theta}{2} - i\alpha_0 \sin \frac{\theta}{2} \right)|\bar{1}\rangle, \quad (20)$$

$$U_{ZZ}(\Theta)(\alpha_{00}|\bar{0}\rangle|\bar{0}\rangle + \alpha_{01}|\bar{0}\rangle|\bar{1}\rangle + \alpha_{10}|\bar{1}\rangle|\bar{0}\rangle + \alpha_{11}|\bar{1}\rangle|\bar{1}\rangle) = e^{-i\Theta/2}(\alpha_{00}|\bar{0}\rangle|\bar{0}\rangle + \alpha_{11}|\bar{1}\rangle|\bar{1}\rangle) + e^{i\Theta/2}(\alpha_{01}|\bar{0}\rangle|\bar{1}\rangle + \alpha_{10}|\bar{1}\rangle|\bar{0}\rangle).$$

The single-qubit rotation $R_Z(\phi)$ can be implemented by external driving described by the following Hamiltonian:

$$H_Z(t) = E_{in}(t)(a + a^\dagger). \quad (21)$$

In the coherent-state basis, this Hamiltonian is represented as a diagonal matrix with eigenvalues $\pm 2E_{in}(t)\alpha_S$. Thus, the two states acquire opposite phases via quantum adiabatic evolution with a pulse-shaped $E_{in}(t)$, and hence $R_Z(\phi)$ is realized.

Similarly, the two-qubit gate $U_{ZZ}(\Theta)$ can be implemented by time-dependent linear coupling:

$$H_{ZZ} = g(t)(a_1 a_2^\dagger + a_1^\dagger a_2). \quad (22)$$

Here, $|\alpha_S\rangle|\alpha_S\rangle$ and $|-\alpha_S\rangle|-\alpha_S\rangle$ acquire phases opposite to those for $|-\alpha_S\rangle|\alpha_S\rangle$ and $|\alpha_S\rangle|-\alpha_S\rangle$ via quantum adiabatic evolution with a pulse-shaped $g(t)$, and hence $U_{ZZ}(\Theta)$ is realized.

Finally, $R_X(\theta)$ is implemented by controlling the detuning as follows. First, Eq. (20) is rewritten as

$$R_X(\theta) \left[\frac{\alpha_0 + \alpha_1}{2}(|\bar{0}\rangle + |\bar{1}\rangle) + \frac{\alpha_0 - \alpha_1}{2}(|\bar{0}\rangle - |\bar{1}\rangle) \right] = \frac{\alpha_0 + \alpha_1}{2}e^{-i\theta/2}(|\bar{0}\rangle + |\bar{1}\rangle) + \frac{\alpha_0 - \alpha_1}{2}e^{i\theta/2}(|\bar{0}\rangle - |\bar{1}\rangle). \quad (23)$$

Note that $|\bar{0}\rangle \pm |\bar{1}\rangle$ are even and odd cat states. By increasing the detuning slowly, even and odd cat states change adiabatically to vacuum and single-photon states, respectively. During this adiabatic process, the cat states acquire different phases depending on the energy gap between the two states. Thus, $R_X(\theta)$ is realized.

From the simulation results reported in Ref. 84, the infidelities of $R_Z(\phi)$, $R_X(\theta)$, and $U_{ZZ}(\Theta)$ are lower than 0.03, 0.003, and 0.06%, respectively, where the gate times are $2K^{-1}$, $10K^{-1}$, and $2K^{-1}$, respectively, and the average photon number for each qubit is 4 in all the cases. These results are obtained assuming no loss in KPOs, which is the dominant decoherence source in this scheme. When there exists such loss, the probability for single-photon loss during a quantum gate operation is given by $\kappa T_g \alpha_S^2$, where κ is the energy decay rate for each KPO, T_g is the gate time, and α_S^2 is the average photon number in each KPO. Since T_g is inversely proportional to K , as shown above, κ must be much smaller than K for achieving a small error probability required for fault-tolerant quantum computation.

6. Summary and Outlook

We have explained theoretical aspects of KPOs and

quantum computers with KPOs (quantum bifurcation machines or QbMs), comparing them with their dissipative counterparts, namely, OPOs and CIMs. KPOs can generate Schrödinger cat states deterministically via quantum adiabatic bifurcations increasing the pumping rate gradually. Two coupled KPOs can yield entangled coherent states (two-mode cat states). KPO networks (QbMs) can solve the Ising problem via quantum adiabatic evolution and also can perform gate-based universal quantum computation. Superconducting-circuit implementations of a KPO and QbMs have also been presented. They offer a new application of Josephson parametric oscillators (JPOs).

The first step toward the realization of QbMs is an experimental demonstration of the cat-state generation using a KPO. However, cat states generated inside a KPO are hard to observe directly. For such observation, Goto et al.¹²⁶ have recently proposed a method for on-demand generation of traveling cat states using a KPO. Since the output field from a KPO can be directly measured, this method allows us to demonstrate cat-state generation using a KPO. On-demand generation of traveling cat states has been experimentally demonstrated using superconducting circuits only very recently.¹²⁷ The method with a KPO offers an alternative approach to this challenging task.

Thus, the theoretical proposals of KPOs and QbMs have opened broad possibilities for theoretical and experimental research in the fields of quantum optics, superconducting circuits, and quantum information science.

Acknowledgment This work was partially supported by JST ERATO (Grant No. JPMJER1601).

*hayato1.goto@toshiba.co.jp

- 1) R. Harris, J. Johansson, A. J. Berkley, M. W. Johnson, T. Lanting, S. Han, P. Bunyk, E. Ladizinsky, T. Oh, I. Perminov, E. Tolkacheva, S. Uchaikin, E. M. Chapple, C. Enderud, C. Rich, M. Thom, J. Wang, B. Wilson, and G. Rose, *Phys. Rev. B* **81**, 134510 (2010).
- 2) R. Harris, M. W. Johnson, T. Lanting, A. J. Berkley, J. Johansson, P. Bunyk, E. Tolkacheva, E. Ladizinsky, N. Ladizinsky, T. Oh, F. Cioata, I. Perminov, P. Spear, C. Enderud, C. Rich, S. Uchaikin, M. C. Thom, E. M. Chapple, J. Wang, B. Wilson, M. H. S. Amin, N. Dickson, K. Karimi, B. Macready, C. J. S. Truncik, and G. Rose, *Phys. Rev. B* **82**, 024511 (2010).
- 3) M. W. Johnson, M. H. S. Amin, S. Gildert, T. Lanting, F. Hamze, N. Dickson, R. Harris, A. J. Berkley, J. Johansson, P. Bunyk, E. M. Chapple, C. Enderud, J. P. Hilton, K. Karimi, E. Ladizinsky, N. Ladizinsky, T. Oh, I. Perminov, C. Rich, M. C. Thom, E. Tolkacheva, C. J. S. Truncik, S. Uchaikin, J. Wang, B. Wilson, and G. Rose, *Nature* **473**, 194 (2011).
- 4) T. Lanting, A. J. Przybysz, A. Yu. Smirnov, F. M. Spedalieri, M. H. Amin, A. J. Berkley, R. Harris, F. Altomare, S. Boixo, P. Bunyk, N. Dickson, C. Enderud, J. P. Hilton, E. Hoskinson, M. W. Johnson, E. Ladizinsky, N. Ladizinsky, R. Neufeld, T. Oh, I. Perminov, C. Rich, M. C. Thom, E. Tolkacheva, S. Uchaikin, A. B. Wilson, and G. Rose, *Phys. Rev. X* **4**, 021041 (2014).
- 5) S. Boixo, T. F. Ronnow, S. V. Isakov, Z. Wang, D. Wecker, D. A. Lidar, J. M. Martinis, and M. Troyer, *Nat. Phys.* **10**, 218 (2014).
- 6) V. S. Denchev, S. Boixo, S. V. Isakov, N. Ding, R. Babbush, V. Smelyanskiy, J. Martinis, and H. Neven, *Phys. Rev. X* **6**, 031015 (2016).
- 7) T. Kadowaki and H. Nishimori, *Phys. Rev. E* **58**, 5355 (1998).
- 8) J. Brooke, D. Bitko, T. F. Rosenbaum, and G. Aeppli, *Science* **284**, 779 (1999).
- 9) G. E. Santoro, R. Martoňák, E. Tosatti, and R. Car, *Science* **295**, 2427 (2002).

- 10) A. Das and B. K. Chakrabarti, *Rev. Mod. Phys.* **80**, 1061 (2008).
11) E. Farhi, J. Goldstone, S. Gutmann, and M. Sipser, [arXiv:quant-ph/0001106](https://arxiv.org/abs/quant-ph/0001106).
12) E. Farhi, J. Goldstone, S. Gutmann, J. Lapan, A. Lundgren, and D. Preda, *Science* **292**, 472 (2001).
13) W. M. Kaminsky, S. Lloyd, and T. P. Orlando, [arXiv:quant-ph/0403090](https://arxiv.org/abs/quant-ph/0403090).
14) M. H. S. Amin, P. J. Love, and C. J. S. Truncik, *Phys. Rev. Lett.* **100**, 060503 (2008).
15) T. Albash and D. A. Lidar, *Rev. Mod. Phys.* **90**, 015002 (2018).
16) F. Barahona, *J. Phys. A* **15**, 3241 (1982).
17) A. Lucas, *Front. Phys.* **2**, 5 (2014).
18) F. Barahona, M. Grötschel, M. Jünger, and G. Reinelt, *Oper. Res.* **36**, 493 (1988).
19) A. Perdomo, C. Truncik, I. Tubert-Brohman, G. Rose, and A. Aspuru-Guzik, *Phys. Rev. A* **78**, 012320 (2008).
20) A. Perdomo-Ortiz, N. Dickson, M. Drew-Brook, G. Rose, and A. Aspuru-Guzik, *Sci. Rep.* **2**, 571 (2012).
21) R. Y. Li, R. D. Felice, R. Rohs, and D. A. Lidar, *npj Quantum Inf.* **4**, 14 (2018).
22) H. Neven, V. S. Denchev, G. Rose, and W. G. Macready, [arXiv:0811.0416](https://arxiv.org/abs/0811.0416).
23) H. Neven, V. S. Denchev, G. Rose, and W. G. Macready, [arXiv:0912.0779](https://arxiv.org/abs/0912.0779).
24) E. G. Rieffel, D. Venturelli, B. O’Gorman, M. B. Do, E. M. Prystay, and V. N. Smelyanskiy, *Quantum Inf. Process.* **14**, 1 (2015).
25) D. Venturelli, D. J. J. Marchand, and G. Rojo, [arXiv:1506.08479](https://arxiv.org/abs/1506.08479).
26) H. Sakaguchi, K. Ogata, T. Isomura, S. Utsunomiya, Y. Yamamoto, and K. Aihara, *Entropy* **18**, 365 (2016).
27) G. Rosenberg, P. Haghnegahdar, P. Goddard, P. Carr, K. Wu, and M. López de Prado, *IEEE J. Sel. Top. Signal Process.* **10**, 1053 (2016).
28) F. Neukart, G. Compostella, C. Seidel, D. von Dollen, S. Yarkoni, and B. Parney, *Frontiers in ICT* **4**, 29 (2017).
29) S. Utsunomiya, K. Takata, and Y. Yamamoto, *Opt. Express* **19**, 18091 (2011).
30) K. Takata, S. Utsunomiya, and Y. Yamamoto, *New J. Phys.* **14**, 013052 (2012).
31) K. Takata and Y. Yamamoto, *Phys. Rev. A* **89**, 032319 (2014).
32) S. Utsunomiya, N. Namekata, K. Takata, D. Akamatsu, S. Inoue, and Y. Yamamoto, *Opt. Express* **23**, 6029 (2015).
33) Z. Wang, A. Marandi, K. Wen, R. L. Byer, and Y. Yamamoto, *Phys. Rev. A* **88**, 063853 (2013).
34) A. Marandi, Z. Wang, K. Takata, R. L. Byer, and Y. Yamamoto, *Nat. Photonics* **8**, 937 (2014).
35) K. Takata, A. Marandi, R. Hamerly, Y. Haribara, D. Maruo, S. Tamate, H. Sakaguchi, S. Utsunomiya, and Y. Yamamoto, *Sci. Rep.* **6**, 34089 (2016).
36) H. Takesue and T. Inagaki, *Opt. Lett.* **41**, 4273 (2016).
37) T. Inagaki, Y. Haribara, K. Igarashi, T. Sonobe, S. Tamate, T. Honjo, A. Marandi, P. L. McMahon, T. Umeki, K. Enbusu, O. Tadanaga, H. Takenouchi, K. Aihara, K. Kawarabayashi, K. Inoue, S. Utsunomiya, and H. Takesue, *Science* **354**, 603 (2016).
38) P. L. McMahon, A. Marandi, Y. Haribara, R. Hamerly, C. Langrock, S. Tamate, T. Inagaki, H. Takesue, S. Utsunomiya, K. Aihara, R. L. Byer, M. M. Fejer, H. Mabuchi, and Y. Yamamoto, *Science* **354**, 614 (2016).
39) Y. Haribara, Y. Yamamoto, K. Kawarabayashi, and S. Utsunomiya, [arXiv:1501.07030](https://arxiv.org/abs/1501.07030).
40) Y. Haribara, S. Utsunomiya, and Y. Yamamoto, *Entropy* **18**, 151 (2016).
41) Y. Haribara, H. Ishikawa, S. Utsunomiya, K. Aihara, and Y. Yamamoto, *Quantum Sci. Technol.* **2**, 044002 (2017).
42) K. Takata, A. Marandi, and Y. Yamamoto, *Phys. Rev. A* **92**, 043821 (2015).
43) A. Yamamura, K. Aihara, and Y. Yamamoto, *Phys. Rev. A* **96**, 053834 (2017).
44) T. Shoji, K. Aihara, and Y. Yamamoto, *Phys. Rev. A* **96**, 053833 (2017).
45) Y. Yamamoto, K. Aihara, T. Leleu, K. Kawarabayashi, S. Kako, M. Fejer, K. Inoue, and H. Takesue, *npj Quantum Inf.* **3**, 49 (2017).
46) I. Mahboob, H. Okamoto, and H. Yamaguchi, *Sci. Adv.* **2**, e1600236 (2016).
47) M. Yamaoka, C. Yoshimura, M. Hayashi, T. Okuyama, H. Aoki, and H. Mizuno, *IEEE J. Solid-State Circuits* **51**, 303 (2016).
48) K. Mizushima, H. Goto, and R. Sato, *Appl. Phys. Lett.* **111**, 172406 (2017).
49) E. Goto, *Proc. IRE* **47**, 1304 (1959).
50) H. Goto, *Sci. Rep.* **6**, 21686 (2016).
51) U. Leonhardt, *Measuring the Quantum State of Light* (Cambridge University Press, Cambridge, U.K., 1997).
52) S. Haroche, *Rev. Mod. Phys.* **85**, 1083 (2013).
53) D. J. Wineland, *Rev. Mod. Phys.* **85**, 1103 (2013).
54) A. Ourjoutsev, R. Tualle-Brouri, J. Laurat, and P. Grangier, *Science* **312**, 83 (2006).
55) A. Ourjoutsev, H. Jeong, R. Tualle-Brouri, and P. Grangier, *Nature* **448**, 784 (2007).
56) S. Deléglise, I. Dotsenko, C. Sayrin, J. Bernu, M. Brune, J.-M. Raimond, and S. Haroche, *Nature* **455**, 510 (2008).
57) B. Vlastakis, G. Kirchmair, Z. Leghtas, S. E. Nigg, L. Frunzio, S. M. Girvin, M. Mirrahimi, M. H. Devoret, and R. J. Schoelkopf, *Science* **342**, 607 (2013).
58) Z. Leghtas, S. Touzard, I. M. Pop, A. Kou, B. Vlastakis, A. Petrenko, K. M. Sliwa, A. Narla, S. Shankar, M. J. Hatridge, M. Reagor, L. Frunzio, R. J. Schoelkopf, M. Mirrahimi, and M. H. Devoret, *Science* **347**, 853 (2015).
59) C. Wang, Y. Y. Gao, P. Reinhold, R. W. Heeres, N. Ofek, K. Chou, C. Axline, M. Reagor, J. Blumoff, K. M. Sliwa, L. Frunzio, S. M. Girvin, L. Jiang, M. Mirrahimi, M. H. Devoret, and R. J. Schoelkopf, *Science* **352**, 1087 (2016).
60) D. V. Sychev, A. E. Ulanov, A. A. Pushkina, M. W. Richards, I. A. Fedorov, and A. I. Lvovsky, *Nat. Photonics* **11**, 379 (2017).
61) S. Puri, C. K. Andersen, A. L. Grimsmo, and A. Blais, *Nat. Commun.* **8**, 15785 (2017).
62) H. Goto, Z. Lin, and Y. Nakamura, *Sci. Rep.* **8**, 7154 (2018).
63) M. H. Amin, E. Andriyash, J. Rolfe, B. Kulchytskyy, and R. Melko, *Phys. Rev. X* **8**, 021050 (2018).
64) G. Kirchmair, B. Vlastakis, Z. Leghtas, S. E. Nigg, H. Paik, E. Ginossar, M. Mirrahimi, L. Frunzio, S. M. Girvin, and R. J. Schoelkopf, *Nature* **495**, 205 (2013).
65) M. Rehák, P. Neilinger, M. Grajcar, G. Oelsner, U. Hübner, E. Il’ichev, and H.-G. Meyer, *Appl. Phys. Lett.* **104**, 162604 (2014).
66) T. Yamamoto, K. Inomata, M. Watanabe, K. Matsuba, T. Miyazaki, W. D. Oliver, Y. Nakamura, and J. S. Tsai, *Appl. Phys. Lett.* **93**, 042510 (2008).
67) J. Bourassa, F. Beaudoin, J. M. Gambetta, and A. Blais, *Phys. Rev. A* **86**, 013814 (2012).
68) W. Wustmann and V. Shumeiko, *Phys. Rev. B* **87**, 184501 (2013).
69) P. Krantz, Y. Reshitnyk, W. Wustmann, J. Bylander, S. Gustavsson, W. D. Oliver, T. Duty, V. Shumeiko, and P. Delsing, *New J. Phys.* **15**, 105002 (2013).
70) C. Eichler and A. Wallraff, *EPJ Quantum Technology* **1**, 2 (2014).
71) Z. R. Lin, K. Inomata, K. Koshino, W. D. Oliver, Y. Nakamura, J. S. Tsai, and T. Yamamoto, *Nat. Commun.* **5**, 4480 (2014).
72) P. Krantz, A. Bengtsson, M. Simoen, S. Gustavsson, V. Shumeiko, W. D. Oliver, C. M. Wilson, P. Delsing, and J. Bylander, *Nat. Commun.* **7**, 11417 (2016).
73) S. E. Nigg, N. Lörch, and R. P. Tiwari, *Sci. Adv.* **3**, e1602273 (2017).
74) W. Lechner, P. Hauke, and P. Zoller, *Sci. Adv.* **1**, e1500838 (2015).
75) A. Rocchetto, S. C. Benjamin, and Y. Li, *Sci. Adv.* **2**, e1601246 (2016).
76) N. Chancellor, S. Zohren, and P. A. Warburton, *npj Quantum Inf.* **3**, 21 (2017).
77) M. Leib, P. Zoller, and W. Lechner, *Quantum Sci. Technol.* **1**, 015008 (2016).
78) P. Zhao, Z. Jin, P. Xu, X. Tan, H. Yu, and Y. Yu, *Phys. Rev. Appl.* **10**, 024019 (2018).
79) M. Dykman, in *Fluctuating Nonlinear Oscillators*, ed. M. Dykman (Oxford University Press, Oxford, U.K., 2012) p. 165.
80) M. Marthaler and M. I. Dykman, *Phys. Rev. A* **73**, 042108 (2006).
81) M. I. Dykman, M. Marthaler, and V. Peano, *Phys. Rev. A* **83**, 052115 (2011).
82) M. I. Dykman, C. Bruder, N. Lörch, and Y. Zhang, [arXiv:1805.12545](https://arxiv.org/abs/1805.12545).
83) D. J. C. MacKay, *Information Theory, Inference and Learning Algorithms* (Cambridge University Press, Cambridge, U.K., 2003).
84) H. Goto, *Phys. Rev. A* **93**, 050301(R) (2016).
85) S. Puri, S. Boutin, and A. Blais, *npj Quantum Inf.* **3**, 18 (2017).

- 86) S. E. Nigg, *Phys. Rev. A* **89**, 022340 (2014).
- 87) M. Mirrahimi, Z. Leghtas, V. V. Albert, S. Touzard, R. J. Schoelkopf, L. Jiang, and M. H. Devoret, *New J. Phys.* **16**, 045014 (2014).
- 88) V. V. Albert, C. Shu, S. Krastanov, C. Shen, R.-B. Liu, Z.-B. Yang, R. J. Schoelkopf, M. Mirrahimi, M. H. Devoret, and L. Jiang, *Phys. Rev. Lett.* **116**, 140502 (2016).
- 89) N. Ofek, A. Petrenko, R. Heeres, P. Reinhold, Z. Leghtas, B. Vlastakis, Y. Liu, L. Frunzio, S. M. Girvin, L. Jiang, M. Mirrahimi, M. H. Devoret, and R. J. Schoelkopf, *Nature* **536**, 441 (2016).
- 90) Y. Zhang, X. Zhao, Z.-F. Zheng, L. Yu, Q.-P. Su, and C.-P. Yang, *Phys. Rev. A* **96**, 052317 (2017).
- 91) S. Rosenblum, Y. Y. Gao, P. Reinhold, C. Wang, C. J. Axline, L. Frunzio, S. M. Girvin, L. Jiang, M. Mirrahimi, M. H. Devoret, and R. J. Schoelkopf, *Nat. Commun.* **9**, 652 (2018).
- 92) K. S. Chou, J. Z. Blumo, C. S. Wang, P. C. Reinhold, C. J. Axline, Y. Y. Gao, L. Frunzio, M. H. Devoret, L. Jiang, and R. J. Schoelkopf, *arXiv:1801.05283*.
- 93) S. Puri, A. Grimm, P. Campagne-Ibarcq, A. Eickbusch, K. Noh, G. Roberts, L. Jiang, M. Mirrahimi, M. H. Devoret, and S. M. Girvin, *arXiv:1807.09334*.
- 94) S. Rosenblum, P. Reinhold, M. Mirrahimi, L. Jiang, L. Frunzio, and R. J. Schoelkopf, *Science* **361**, 266 (2018).
- 95) M. Bremner, R. Jozsa, and D. Shepherd, *Proc. R. Soc. London, Ser. A* **467**, 459 (2011).
- 96) S. H. Strogatz, *Nonlinear Dynamics and Chaos* (Westview Press, Boulder, CO, 2015) 2nd ed.
- 97) L. D. Landau and E. M. Lifshitz, *Mechanics* (Butterworth, Oxford, U.K., 1976) 3rd ed.
- 98) H. Goldstein, C. Poole, and J. Safko, *Classical Mechanics* (Addison-Wesley, New York, 2000) 3rd ed.
- 99) V. I. Arnold, *Mathematical Methods of Classical Mechanics* (Springer, Berlin/Heidelberg, 1989) 2nd ed.
- 100) D. F. Walls and G. J. Milburn, *Quantum Optics* (Springer, Berlin, 1994).
- 101) S. Touzard, A. Grimm, Z. Leghtas, S. O. Mundhada, P. Reinhold, C. Axline, M. Reagor, K. Chou, J. Blumoff, K. M. Sliwa, S. Shankar, L. Frunzio, R. J. Schoelkopf, M. Mirrahimi, and M. H. Devoret, *Phys. Rev. X* **8**, 021005 (2018).
- 102) Y. Zhang and M. I. Dykman, *Phys. Rev. A* **95**, 053841 (2017).
- 103) H.-P. Breuer and F. Petruccione, *The Theory of Open Quantum Systems* (Oxford University Press, Oxford, U.K., 2002).
- 104) H. J. Carmichael, in *An Open Systems Approach to Quantum Optics*, ed. W. Beiglböck (Springer, Berlin, 1993) Lecture Notes in Physics, Vol. 18.
- 105) M. B. Plenio and P. L. Knight, *Rev. Mod. Phys.* **70**, 101 (1998).
- 106) J. Koch, T. M. Yu, J. Gambetta, A. A. Houck, D. I. Schuster, J. Majer, A. Blais, M. H. Devoret, S. M. Girvin, and R. J. Schoelkopf, *Phys. Rev. A* **76**, 042319 (2007).
- 107) D. I. Schuster, A. A. Houck, J. A. Schreier, A. Wallraff, J. M. Gambetta, A. Blais, L. Frunzio, J. Majer, B. Johnson, M. H. Devoret, S. M. Girvin, and R. J. Schoelkopf, *Nature* **445**, 515 (2007).
- 108) J. Majer, J. M. Chow, J. M. Gambetta, J. Koch, B. R. Johnson, J. A. Schreier, L. Frunzio, D. I. Schuster, A. A. Houck, A. Wallraff, A. Blais, M. H. Devoret, S. M. Girvin, and R. J. Schoelkopf, *Nature* **449**, 443 (2007).
- 109) A. A. Houck, D. I. Schuster, J. M. Gambetta, J. A. Schreier, B. R. Johnson, J. M. Chow, J. Majer, L. Frunzio, M. H. Devoret, S. M. Girvin, and R. J. Schoelkopf, *Nature* **449**, 328 (2007).
- 110) J. M. Fink, M. Göppel, M. Baur, R. Bianchetti, P. J. Leek, A. Blais, and A. Wallraff, *Nature* **454**, 315 (2008).
- 111) L. DiCarlo, J. M. Chow, J. M. Gambetta, L. S. Bishop, B. R. Johnson, D. I. Schuster, J. Majer, A. Blais, L. Frunzio, S. M. Girvin, and R. J. Schoelkopf, *Nature* **460**, 240 (2009).
- 112) L. DiCarlo, D. Reed, L. Sun, B. R. Johnson, J. M. Chow, J. M. Gambetta, L. Frunzio, S. M. Girvin, M. H. Devoret, and R. J. Schoelkopf, *Nature* **467**, 574 (2010).
- 113) M. D. Reed, L. DiCarlo, S. E. Nigg, L. Sun, L. Frunzio, S. M. Girvin, and R. J. Schoelkopf, *Nature* **482**, 382 (2012).
- 114) R. Barends, J. Kelly, A. Megrant, D. Sank, E. Jeffrey, Y. Chen, Y. Yin, B. Chiaro, J. Mutus, C. Neill, P. O’Malley, P. Roushan, J. Wenner, T. C. White, A. N. Cleland, and J. M. Martinis, *Phys. Rev. Lett.* **111**, 080502 (2013).
- 115) R. Barends, J. Kelly, A. Megrant, A. Veitia, D. Sank, E. Jeffrey, T. C. White, J. Mutus, A. G. Fowler, B. Campbell, Y. Chen, Z. Chen, B. Chiaro, A. Dunsworth, C. Neill, P. O’Malley, P. Roushan, A. Vainsencher, J. Wenner, A. N. Korotkov, A. N. Cleland, and J. M. Martinis, *Nature* **508**, 500 (2014).
- 116) J. Kelly, R. Barends, A. G. Fowler, A. Megrant, E. Jeffrey, T. C. White, D. Sank, J. Y. Mutus, B. Campbell, Y. Chen, Z. Chen, B. Chiaro, A. Dunsworth, I.-C. Hoi, C. Neill, P. J. J. O’Malley, C. Quintana, P. Roushan, A. Vainsencher, J. Wenner, A. N. Cleland, and J. M. Martinis, *Nature* **519**, 66 (2015).
- 117) J. M. Martinis and K. Osborne, *arXiv:cond-mat/0402415*.
- 118) M. Tinkham, *Introduction to Superconductivity* (McGraw-Hill, New York, 1996) 2nd ed.
- 119) Y. Makhlin, G. Schön, and A. Shnirman, *Rev. Mod. Phys.* **73**, 357 (2001).
- 120) V. V. Ryazanov, V. A. Oboznov, A. Y. Rusanov, A. V. Veretennikov, A. A. Golubov, and J. Aarts, *Phys. Rev. Lett.* **86**, 2427 (2001).
- 121) T. Kontos, M. Aprili, J. Lesueur, F. Genêt, B. Stephanidis, and R. Boursier, *Phys. Rev. Lett.* **89**, 137007 (2002).
- 122) E. C. Gingrich, B. M. Niedzielski, J. A. Glick, Y. Wang, D. L. Miller, R. Loloei, W. P. Pratt, Jr., and N. O. Birge, *Nat. Phys.* **12**, 564 (2016).
- 123) V. Choi, *Quantum Inf. Process.* **7**, 193 (2008).
- 124) V. Choi, *Quantum Inf. Process.* **10**, 343 (2011).
- 125) M. A. Nielsen and I. L. Chuang, *Quantum Computation and Quantum Information* (Cambridge University Press, Cambridge, U.K., 2000).
- 126) H. Goto, Z. Lin, T. Yamamoto, and Y. Nakamura, *arXiv:1808.03003*.
- 127) W. Pfaff, C. J. Axline, L. D. Burkhardt, U. Vool, P. Reinhold, L. Frunzio, L. Jiang, M. H. Devoret, and R. J. Schoelkopf, *Nat. Phys.* **13**, 882 (2017).



Hayato Goto was born in Shizuoka, Japan in 1978. He obtained his B.Sc. (2001) and M.Sc. (2003) degrees from the University of Tokyo. Since 2003, he has been a researcher at the Corporate Research & Development Center, Toshiba Corporation. In 2007, he obtained his Ph.D. degree from the University of Tokyo. He worked on optical experiments with optical parametric oscillators and rare-earth-ion-doped crystals toward their applications to quantum information processing. He has recently worked on quantum computation with nonlinear oscillators and theories of fault-tolerant quantum computation. His current interest is in the realization of quantum computers using superconducting circuits.